Phase Space Theory of Evaporation in Neon Clusters: The Role of Quantum Effects[†]

F. Calvo*

LASIM, Université Claude Bernard Lyon 1 and CNRS UMR 5579, Bat. A. Kastler, 43 Bd du 11 novembre 1918, F69622 Villeurbanne, France

P. Parneix

LPPM, Fédération Lumière-Matière, CNRS and Université Paris-Sud, F91405 Orsay Cedex, France

Received: April 9, 2009; Revised Manuscript Received: May 29, 2009

Unimolecular evaporation of neon clusters containing between 14 and 148 atoms is theoretically investigated in the framework of phase space theory. Quantum effects are incorporated in the vibrational densities of states, which include both zero-point and anharmonic contributions, and in the possible tunneling through the centrifugal barrier. The evaporation rates, kinetic energy released, and product angular momentum are calculated as a function of excess energy or temperature in the parent cluster and compared to the classical results. Quantum fluctuations are found to generally increase both the kinetic energy released and the angular momentum of the product, but the effects on the rate constants depend nontrivially on the excess energy. These results are interpreted as due to the very few vibrational states available in the product cluster when described quantum mechanically. Because delocalization also leads to much narrower thermal energy distributions, the variations of evaporation observables as a function of canonical temperature appear much less marked than in the microcanonical ensemble. While quantum effects tend to smooth the caloric curve in the product cluster, the melting phase change clearly keeps a signature on these observables. The microcanonical temperature extracted from fitting the kinetic energy released distribution using an improved Arrhenius form further suggests a backbending in the quantum Ne_{13} cluster that is absent in the classical system. Finally, in contrast to delocalization effects, quantum tunneling through the centrifugal barrier does not play any appreciable role on the evaporation kinetics of these rather heavy clusters.

I. Introduction

The quantum dynamics of many-body molecular systems remains a major challenge in theoretical physical chemistry. While the classical Hamilton equations of motion can be accurately solved numerically for very large systems and over long time scales, the solution of the time-dependent Schrödinger equation is only available in low dimensions.[1] Practical schemes to address the quantum dynamics include time-dependent self-consistent field and configuration interaction,[2] multiconfigurational extensions,[3] path-integral based methods such as centroid[4] and ring−polymer[5] molecular dynamics, coherent state expansions,[6] Bohmian methods,[7,8] and related schemes[9] as well as Gaussian variational wave packets.[10−12] Some methods such as ab initio multiple spawning[13] or multiconfigurational nuclear-electronic orbital[14] have been designed to address vibrational and electronic degrees of freedom on a common quantum mechanical ground. For moderately quantum systems or for hybrid quantum/classical systems, perturbative methods,[15] and other semiclassical approaches have been proposed.[16−21] The relative merits of these different methods are discussed in review articles.[22] Several of them, such as those based on path integrals, are specifically appropriate for condensed matter problems, because they are naturally formulated in the canonical ensemble of statistical mechanics.[23] Gas-phase systems, on the other hand, are better described at constant total energy. The zero-point energy constrained trajectory method of Bowman, Miller, Keyes, and co-workers,[24−26] which extends the quasiclassical trajectory model[27] and has been subsequently improved by various authors,[28−31] becomes numerically involved in high-dimensional systems and vulnerable to instabilities in anharmonic regions. Unfortunately, the more rigorous wave packet propagation schemes also suffer heavily from such problems, as discussed in detail by Buch in the case of Gaussian variational wave packets.[12]

The thermal fragmentation of an isolated atomic cluster is a typical situation involving strong anharmonicities, long time scales, and whose description clearly pertains to the microcanonical ensemble: except in the limit of large systems, evaporative cooling is expected to change significantly the cluster temperature upon dissociation. Fragmentation is a very important process in the physics and chemistry of clusters, as it gives access to many fundamental properties ranging from binding energies[32] to temperatures[33,34] and even entire caloric curves.[35,36] Statistical theories play a key role in interpreting such experimental measurements. However, these theories usually contain adjustable parameters, and their reliability is very difficult to assess based on experiment only. Molecular dynamics simulations can be carried out in *classical* systems that can be modeled using explicit potential energy surfaces.[37−40] From these "numerically exact" calculations, theories based on the microreversibility principle were shown to be quite accurate for predicting dissociation related properties, namely kinetic energies released (KERs), angular momentum, and their probability distributions, as well as rate constants.[39−42] These approaches, particularly the orbiting

[†] Part of the "Vincenzo Aquilanti Festschrift".

* Corresponding author.

10.1021/jp903282b
Published on Web 07/02/2009

transition state version of phase space theory (PST),[43−47] can also be expressed for quantum systems, as was originally proposed in chemical reaction kinetics.[43,44] However, their application to polyatomic systems becomes combinatorially cumbersome due to the difficulty of calculating rotational and vibrational densities of states in high-dimensional manifolds. Interestingly, strongly quantum systems such as helium droplets could be treated using dedicated, fluidlike approximations owing to the loss of geometric structure.[48,49] Moderately quantum systems have also been investigated through statistical theories using ad hoc semiclassical corrections on top of classical calculations.[40]

Neon clusters are expected to have a significant quantum character. This is for instance indicated by the de Boer parameter $\Lambda = \hbar\sigma/(m\varepsilon)^{1/2} \approx 0.1$, which quantifies the extent of quantum delocalization based on the atomic mass m, the equilibrium distance σ, and well depth ε of the interaction potential. Quantum effects in neon clusters have been illustrated on the frequent changes in stable structures due to zero-point vibrational motion[9,50,51] and on the depression on the melting point.[50,52−56] In condensed phases, quantum effects also alter structural and dynamical properties to an appreciable amount.[57,58] The present work focuses on evaporation kinetics of medium-size neon clusters, for which we have chosen a purely statistical PST description rather than an explicit but problematic dynamical modeling. We build here upon the success of the PST framework in reproducing atomistic results in classical clusters of similar complexity[39−41] and make the assumption that phase space theory will be sufficiently accurate for addressing the quantum clusters as well. Our incorporation of quantum effects within PST is 2-fold. Vibrational densities of states are calculated using the superposition approximation,[50,59] which takes into account both intrabasin anharmonicities and the fluxional character of the clusters, as well as quantum delocalization and zero-point energies. Tunneling, though neglected in the evaluation of vibrational densities of states, is included semiclassically in the calculation of the rotational densities. Our results show a strong influence of quantum delocalization on evaporation related observables, which cannot be captured by simple quantum corrections to the classical theory. In particular, the very few vibrational states available at low excess energy lead to an increase in both the kinetic energy released and the angular momentum of the product cluster. However, the picture somewhat changes when temperature is chosen as the control variable, quantum effects generally decreasing down to being minor corrections. Yet, the melting phase change in the product cluster keeps a clear signature on the dissociation properties in the quantum case, with the expected depression in the melting point.

The article is organized as follows. In the next section, the main elements of phase space theory that are relevant to the present system are briefly described, along with the methods employed to compute the quantum densities of vibrational and rotational states. The application to neon clusters is presented and discussed in section III, with a special emphasis on the Ne_{14} parent, for which we were able to quantify the importance of anharmonicities. Larger clusters containing 56 and 148 atoms are also considered but at the simpler harmonic level. We finally summarize and give some concluding remarks in section IV.

II. Methods

Our theoretical modeling of cluster evaporation is based on phase space theory in its orbiting transition state version, and follows the lines of Chesnavich and Bowers[47] in their treatment of angular momentum constraints. However, for the sake of simplicity we will assume that the parent cluster is nonrotating. For the unimolecular evaporation $Ne_{n+1} \rightarrow Ne_n + Ne$, we denote by E_0 the dissociation energy, which possibly includes a zero-point contribution, and E the excess energy of the parent Ne_{n+1}. For each evaporation event, the translational and rotational kinetic energies of the product cluster, as well as their sum, are denoted as ε_t, ε_r, and ε_{tr}, respectively. The product angular momentum J_r exactly compensates the orbital momentum L. Neon clusters are modeled using a simple pairwise Lennard-Jones (LJ) potential with well depth 35.8 K and distance parameter $\sigma = 2.75$ Å. In the following, atomic units are used throughout unless specified otherwise.

A. Phase Space Theory for Classical and Quantum Clusters. The orbiting transition state version of phase space theory assumes that the dissociation products are the transition state.[47] The probability that an evaporation event at excess energy E releases the kinetic energy ε_{tr} is given by the differential rate $R(E,\varepsilon_{tr})$,

$$R(E,\varepsilon_{tr}) = \frac{g\Omega_n(E - E_0 - \varepsilon_{tr})\,\Gamma(\varepsilon_{tr})}{h\Omega_{n+1}(E)} \tag{1}$$

where $\Omega_n(E)$ is the density of vibrational states of cluster Ne_n at excess energy E above the zero-point reference energy, $\Gamma(\varepsilon_{tr})$ is the density of rotational states of the products, that is, the number of rotational states compatible with energy and angular momentum constraints for a given kinetic energy released. The factor g is a so-called channel degeneracy factor,[39] which is taken here as one for simplicity. Degeneracies arising from the symmetries of the product and parent clusters are implicitely included in the absolute densities $\Omega_n(E)$. Treating kinetic energies released as continuous variables (even though angular momentum may be treated as a multiple integer of $\hbar$), the evaporation rate constant $k(E)$ is the sum of the differential rate over all possible values of ε_{tr} and is expressed in the more familiar form $k(E) = W(E)/h\Omega_{n+1}(E)$, with $W(E)$ the sum of states at the (loose) transition state

$$W(E) = \int_0^{E-E_0} \Omega_n(E - E_0 - \varepsilon_{tr})\Gamma(\varepsilon_{tr})\,d\varepsilon_{tr} \tag{2}$$

The equilibrium probability distribution $P(E,\varepsilon_{tr})$ of the total (translational + rotational) KER and the average value $\langle\varepsilon_{tr}\rangle(E)$ are given by[39]

$$P(E,\varepsilon_{tr}) = R(E,\varepsilon_{tr})/\int_0^{E-E_0} R(E,\varepsilon_{tr})\,d\varepsilon_{tr} \tag{3}$$

and

$$\langle\varepsilon_{tr}\rangle(E) = \int_0^{E-E_0} \varepsilon_{tr}P(E,\varepsilon_{tr})\,d\varepsilon_{tr} \tag{4}$$

respectively. The purely translational KER distribution, $P_t(E,\varepsilon_t)$, can also be calculated using the PST formalism, following an expression first obtained by Klots, by an integration over all possible values of the rotational energy ε_r as[45]

$$P_t(E,\varepsilon_t) \propto \int_0^{\varepsilon_r^{max}} \Omega_n(E - E_0 - \varepsilon_t - \varepsilon_r)\frac{\partial\Gamma}{\partial\varepsilon_r}\,d\varepsilon_r \tag{5}$$

Here we have denoted ε_r^{max} the maximum value of the rotational energy available due to angular momentum constraints. Whereas the absolute rate constant $k(E)$ depends on the properties of both the parent and product clusters, the distributions of kinetic energies released are functions of the product properties only. This is valuable, because absolute densities of vibrational states are not easy to calculate.[39,60] Probability distributions and averages thus offer a much more convenient test of the role of quantum effects on the dissociation observables. The main tasks consist now in estimating the key ingredients entering the above equations, namely the vibrational and rotational densities of states, for both quantum and classical systems. Specific methods have been employed for these two quantities, and they are detailed below.

B. Densities of Vibrational States. Densities of vibrational states can be quite conveniently obtained for multidimensional *classical* systems using a combination of simulation methods, and in the present work we have used standard exchange Monte Carlo simulations followed by histogram reweighting.[61] This method only provides state densities to within an unknown factor, and to determine the absolute densities, this factor was adjusted to recover the harmonic limit $\Omega_n^{HC}(E)$ at low energy:

$$\Omega_n^{HC}(E) = S_n \frac{E^{3n-7}}{(3n-7)!(\hbar\bar{\omega}_n)^{3n-6}} \tag{6}$$

Here we denoted $\bar{\omega}_n$ the geometric average of the vibrational frequency taken at the ground state structure (global minimum), and S_n a factor which accounts for distinguishable permutation-inversion isomers corresponding to stationary points with the same structure. If o_n denotes the order of the point group, then $S_n = 2n!/o_n$.

The above method was used to calculate numerically the density of vibrational states of the clusters Ne_{13} and Ne_{14}. The exchange Monte Carlo simulations were carried out using 50 replicas in the canonical ensemble, with a geometric progression for the temperature ladder in the range 0.3−18 K. A rigid wall container with radius 2.5σ was implemented to keep the atoms connected.

This procedure does not apply for quantum systems. Whereas path-integral techniques or quasiclassical effective potentials[62] can be fruitfully used to sample the canonical thermodynamical properties, densities of vibrational states are much more difficult to calculate in general. Inverse Laplace transformation of the partition function remains plagued with numerical problems.[63] Several approximate schemes have been designed to include quantum delocalization as a correction to classical results.[64−67] A particularly popular such scheme is the Pitzer−Gwinn (PG) approximation,[68] which consists of decoupling quantum effects from anharmonicities, by writing the quantum anharmonic partition function $Q_{q,a}$ as the product of a quantum but harmonic function $Q_{q,h}$ with an anharmonic but classical function $Q_{c,a}$, together with a normalizing harmonic classical function $Q_{c,h}$:

$$Q_{q,a} \simeq \frac{Q_{q,h} \times Q_{c,a}}{Q_{c,h}} \tag{7}$$

The PG method has been used previously as an empirical way of correcting for quantum effects in the caloric curves of clusters,[69] and it can also be formulated in the microcanonical ensemble.[70,71] The latter method has been used by Peslherbe and Hase[40] in the context of unimolecular dissociation.

Alternatively, equilibrium properties can be estimated by superposition over many isomers.[72] This superposition approach is formally exact in classical systems, where the configuration space can be entirely partitioned into basins of attractions, and it has been successfully used for describing atomic clusters,[59,73,74] model glass formers[75] and, more recently, biomolecules.[76] In the quantum case, the superposition approach neglects tunneling but accounts for zero-point effects.[50] In its harmonic version, and contrary to path-integral based methods, it is also expected to be more accurate at very low temperatures. The superposition method is used here in the microcanonical ensemble, where it readily yields an estimate of the density of vibrational states $\Omega_n(E)$ from a known set of minima $\{\alpha\}$:[50]

$$\Omega_n(E) = \sum_\alpha S_n^{(\alpha)} \Omega_n^{(\alpha)}(E - E_\alpha)\Theta(E - E_\alpha) \tag{8}$$

in which $\Omega_n^{(\alpha)}$ denotes the density of vibrational states of isomer α, E_α is its minimum energy including the zero-point energy contribution, and Θ is the Heaviside step function. For separable systems, $\Omega_n^{(\alpha)}(E)$ can be obtained by direct counting using the Beyer−Swinehart algorithm.[77] Fully coupled anharmonic systems, on the other hand, require numerical quadrature, e.g., through Monte Carlo methods.[78−80] At the harmonic level, the quantum superposition approximation already performs semi-quantitatively with respect to more accurate path integral calculations.[50] For instance, the depression in the melting point of Ne_{13} due to quantum delocalization is correctly estimated to be about 1 K.[50] However, because evaporation takes place at high energies, anharmonicities are expected to be very important in dissociation properties.

Application of the quantum superposition method was made using a nearly exhaustive database of 1509 isomers for Ne_{13}, but only a restricted sample for Ne_{14}. In the latter case, accounting for the missing isomers can be achieved by re-weighting of the available minima[50,59] at the price of a new factor $w_n^{(\alpha)}$ in eq 8. The original procedure, introduced by Wales for classical systems,[59] also applies to the quantum superposition approximation.[50] For all minima of both Ne_{13} and Ne_{14}, the vibrational frequencies $\{\omega_\alpha^{(i)}\}$ were obtained by diagonalization of the dynamical matrix, and anharmonic corrections were included empirically within a Dunham quadratic expansion. More precisely, the discrete energy levels of isomer α are expressed as a function of the quantum numbers $\{n_i\}$ as

$$E = E_\alpha + \sum_{i=1}^{\kappa} \hbar\omega_\alpha^{(i)}\left(n_i + \frac{1}{2}\right) + \sum_{i=1}^{\kappa} \omega_\alpha^{(i)}\chi_\alpha^{(i)}\left(n_i + \frac{1}{2}\right)^2 \tag{9}$$

$\kappa = 3n - 6$ being the number of vibrational degrees of freedom and $\chi_\alpha^{(i)}$ the anharmonic coefficient of mode i. The problem was further simplified by assuming that $\chi_\alpha^{(i)}$ only depends on the minimum, but not on the frequencies, and only four values were used depending on the rank α. The global minimum structure (rank 1) was given a coefficient χ_1, whereas the other isomers were arbitrarily divided into groups of 10, 100, and all remaining isomers, with coefficients χ_2, χ_3, and χ_4, respectively. These coefficients were then adjusted to reproduce the accurate heat capacities obtained for Ne_{13} by Frantsuzov and Mandelshtam using the imaginary time variational Gaussian wavepacket (GWP) method.[82] A similar procedure was followed for Ne_{14}.[83] After the error minimization problem was solved numerically,

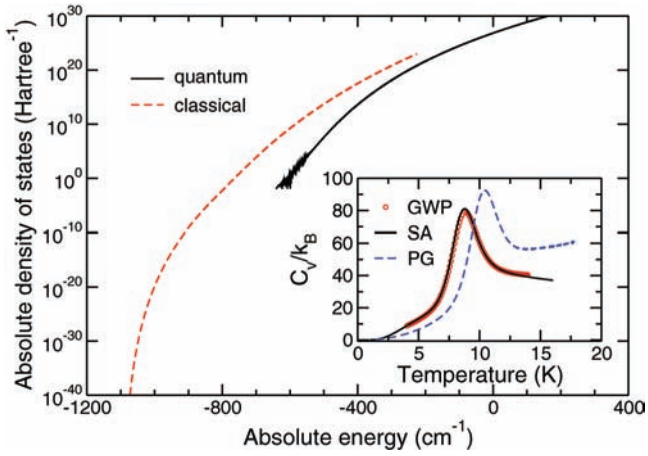

Figure 1. Absolute densities of vibrational states for the Ne_{13} cluster, assuming classical or quantum statistics with full anharmonicities. Inset: canonical heat capacities for the quantum system inferred from the displayed density of states (SA), compared with the predictions of the variational Gaussian wavepacket (GWP) method and with the results of the Pitzer-Gwinn (PG) method.

the quantum densities of states were determined as a function of energy using eq 8, with individual densities $\Omega_n^{(\alpha)}(E)$ obtained using the Beyer−Swinehart method.[77]

The absolute classical and quantum densities of vibrational states are illustrated in Figure 1 for the Ne_{13} cluster. For the classical system, the linear region marks the onset of the solid−liquid phase change, but such behavior is not clearly seen in the quantum system, where fluctuations dominate at low energies. The reliability of quantum density of states is better examined on the canonical heat capacity obtained from the first two moments of energy, $\langle E^p \rangle$ with $p = 1$ or 2, after Laplace transformation:

$$\langle E^p \rangle(T) = \frac{1}{Z(T)} \int E^p \Omega_n(E) \exp(-E/k_B T)\, \mathrm{d}E \qquad (10)$$

$$Z(T) = \int \Omega_n(E) \exp(-E/k_B T)\, \mathrm{d}E \qquad (11)$$

The agreement between the superposition result and the GWP data is very good, but of course not fortuitous. Comparing with the results previously obtained using the superposition method, but with phenomenological anharmonic corrections,[50,84] we find a much better match, especially at low and high temperatures, away from the melting peak. We also show in the inset of Figure 1 the predictions of the Pitzer−Gwinn method for the same cluster. Here the classical anharmonic partition function $Q_{c,a}$ was taken from the classical exchange Monte Carlo simulation, and the ratio $Q_{q,h}/Q_{c,h}$ was calculated using the superposition approximation for both quantum and classical functions. As can be seen from Figure 1, the quantum corrections arising from this method are far unsufficient to reproduce the reference heat capacity. Due to this rather deceptive result, the Pitzer-Gwinn scheme was not given further attention in the present work.

C. Rotational Densities of States and Product Angular Momentum. The rotational densities of states $\Gamma(\varepsilon_{tr})$ entering the PST equations account for the number of states in phase space that are compatible with energy and angular momentum constraints. The total kinetic energy released ε_{tr} is partitioned into its rotational ε_r and translational ε_t components, and we denote by J_r the angular momentum of the product cluster after unimolecular evaporation. For the present icosahedral clusters, the product can be safely considered as spherical, and we denote by B its rotational constant. We restrict here to nonrotating parent clusters, hence the orbital momentum of the reaction exactly compensates J_r.

In *classical* systems, the translational energy must exceed a centrifugal barrier $\varepsilon^\dagger$ arising from orbital momentum. Assuming a simple radial dissociation potential of the form $V(r) = -C_6/r^6$, the height of the centrifugal barrier is $\varepsilon^\dagger(J_r) = J_r^3/\Lambda$ with the parameter $\Lambda = (6\,\mu)^{3/2} C_6^{1/2}/2$. We neglect here some possible corrections due to the finite extent of the product cluster, which could be represented by introducing the radius r_0 such that[39] $V(r) = -C_6/(r - r_0)^6$ or the more tractable form[85] $V(r) = -C_6/r^2(r^2 - r_0^2)^2$. Taking $r_0 = 0$, the corresponding maximum rotational energy available at fixed translational energy ε_t in eq 5 reads $\varepsilon_r^{max}(\varepsilon_t) = \varepsilon_t^{2/3}/\Lambda$. For a given evaporation event, the maximum angular momentum J_r^{max} allowed is such that

$$\varepsilon_{tr} = B(J_r^{max})^2 + \varepsilon^\dagger(J_r^{max}) \qquad (12)$$

which must be solved numerically depending on ε_{tr}. For a spherical product, each value of J_r has a $2J_r$ rotational degeneracy, and the density of rotational states reads[39,47]

$$\Gamma(\varepsilon_{tr}) = \int_0^{J_r^{max}} 2J_r\, \mathrm{d}J_r = (J_r^{max})^2 \qquad (13)$$

In *quantum* systems, J_r becomes a quantum number and a simple semiclassical quantization is performed, rotational energies are expressed as $BJ_r(J_r + 1)$ rather than BJ_r^2. This also affects the centrifugal barrier $\varepsilon^\dagger(J_r)$, which now is $[J_r(J_r + 1)]^{3/2}/\Lambda$. Only multiple values of $\hbar$ are considered for J_r, including J_r^{max}. The rotational density is written as a discrete sum:

$$\Gamma(\varepsilon_{tr}) = \sum_{J_r=0}^{J_r^{max}} (2J_r + 1) \qquad (14)$$

Quantum effects also indirectly enter the previous expressions, through the values of the rotational constants.

1. Rotational Constants. The shapes of the parent and product clusters at their most stable configuration poorly reflect their actual value when dissociation takes place. Temperature leads to strong deformations, which for the present clusters can be simply estimated from Monte Carlo simulations. Effective rotational constants have been determined as their statistical average during constant-temperature MC simulations, using the simple definition based on the arithmetic average of the principal momenta of inertia I_1, I_2, and I_3:

$$\langle B \rangle(T) = \left\langle \left(\frac{1}{2I_1} + \frac{1}{2I_2} + \frac{1}{2I_3} \right)/3 \right\rangle \qquad (15)$$

These effective constants have been obtained for the classical cluster during the same exchange Monte Carlo simulation that was used to calculate the anharmonic densities of states of the product cluster.

In the quantum case, we have performed additional exchange Monte Carlo simulations, but with a modified potential energy surface including quantum corrections based on the quadratic Feynman−Hibbs potential.[62] This approach was previously

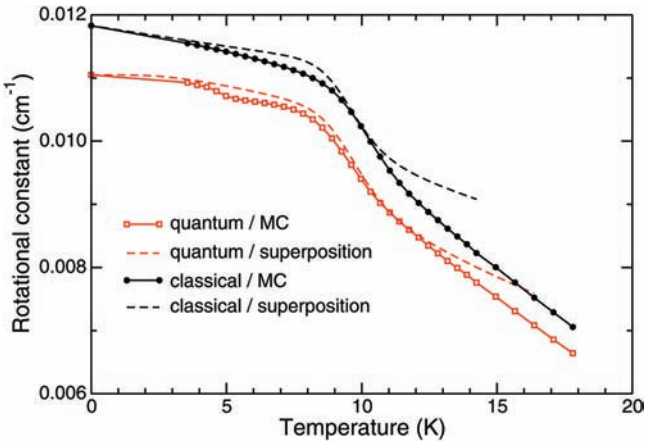

Figure 2. Thermally averaged rotational constant of the Ne_{13} cluster obtained as a function of temperature from classical and quantum-corrected Monte Carlo simulations. Predictions of the harmonic superposition method are also shown.

shown[50] to give thermal equilibrium properties in good agreement with path-integral methods.

In addition to these direct approaches, we have also computed the effective rotational constants using the superposition method in the canonical ensemble. The effective rotational constant is then the sum of all isomer-dependent values, $B_\alpha(T)$, weighed by the canonical partition function of the isomers.[74] Temperature effects on the rotational constant of each isomer are included only through a harmonic approximation, whereas the individual Boltzmann weights incorporate the same anharmonic corrections as used in the microcanonical densities of states. Expressions for the thermally averaged rotational constant B_α are given in the Appendix. In particular, these expressions for the quantum system account for a shift in the ground state 0 K structure due to zero-point effects.

The thermally and isotropically averaged rotational constants resulting from these simulations and from the superposition calculations are represented in Figure 2 for the Ne_{13} cluster. The steady decrease at low temperatures marks the thermal expansion of the cluster, and the soft melting near 9−11 K further leads to a drop in the rotational constant due to the appearance of disordered but more extended structures. In the liquid state, temperature effects approximately results in a 15% decrease in the rotational constant, while quantum effects contribute to another 10%.

The rotational constants obtained by MC simulation are in rather good agreement with the calculations from the superposition method. The location of the melting temperature, in particular, is well reproduced, which is attributed to the correct account of anharmonicities in the partition functions. Some deviations in the slope of $\langle B\rangle(T)$ are found above the melting point, likely due to the neglect of these anharmonicities in the calculation of $B_\alpha(T)$. From Figure 2, we chose to take effective rotational constant of the product cluster as the value at a meaningful temperature, close to the melting point, and to neglect higher-order effects due to the temperature variation of these constants. This approximation will be justified below.

2. Tunneling through the Centrifugal Barrier. The classical restraint $J_r \le J_r^{max}$ does not apply in quantum systems, where the dissociating atom may have tunneled through the centrifugal barrier. Tunneling effects on dissociation and scattering have been mainly studied in the context of ionic fragmentation.[86,87] Here a semiclassical WKB approximation[88] is used to estimate the probability of tunneling events as

$$\chi(\varepsilon_{tr},J_r) = [1 + \exp 2\theta(\varepsilon_{tr},J_r)]^{-1} \tag{16}$$

with the phase integral θ defined by

$$\theta(\varepsilon_{tr},J_r) = \frac{2\pi}{\hbar} \times \int_{r_1}^{r_2}\left[2\mu\left(\frac{J_r(J_r+1)}{2\mu r^2} - \frac{C_6}{r^6} + BJ_r(J_r+1) - \varepsilon_{tr}\right)\right]^{1/2} dr \tag{17}$$

and where r_1 and r_2 denote the lower and upper limits of the radial distance r compatible with the integrand existence. Translational energies, though not quantified, impose $BJ_r(J_r + 1) \le \varepsilon_{tr}$. The quantum density of rotational states is then corrected accordingly from eq 14 to allow for angular momenta higher than J_r^{max} as

$$\Gamma(\varepsilon_{tr}) = \sum_{J_r=0}^{J_r^{max}}(2J_r+1) + \sum_{J_r>J_r^{max}}\chi(\varepsilon_{tr},J_r)(2J_r+1) \tag{18}$$

In practice, and following the work of Larregaray and coworkers,[89] integration is stopped at high values of J_r such that $\chi(\varepsilon_{tr},J_r) < 10^{-3}$. Likewise, eq 5 must be corrected by a second integral over rotational energies higher than ε_r^{max}, but lower than $E - E_0 - \varepsilon_t$, and containing the tunneling factor.

The rotational densities of states have been calculated for the $Ne_{13} + Ne$ system, treating Ne_{13} as a spherical top with rotational constant as discussed in the previous subsection. The variations of Γ with kinetic energy released are represented in Figure 3 for the classical and quantum cases, with a special attention to the tunneling correction to eq 14. The classical density smoothly increases, and approximately varies with ε_{tr} as $\Gamma(\varepsilon_{tr}) \simeq \varepsilon_{tr}(1 - a\varepsilon_{tr}^b)/B_r$. The two coefficients a and b are given by a low-order perturbative expansion of eq 12 as $a = (\Lambda B^{3/2})^{-1}$ and $b = 1/2$. In particular, the large ε_{tr} behavior of $\Gamma \sim \varepsilon_{tr}/B$ converges to the well-known result obtained by Klots for atom + nonlinear polyatomic reactions.[90] The quantum density displays some discrete structure, which essentially follows (but lies above) the classical density. The discrete character reflects that $J_r/\hbar$ can only take integer values, new

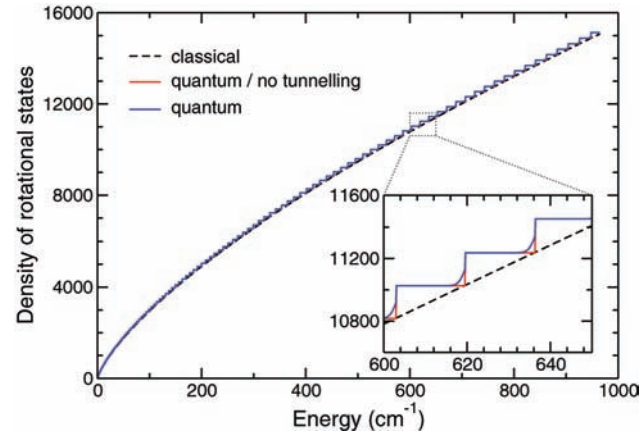

Figure 3. Rotational density of states for the evaporation of an atom from Ne_{14}, treating the Ne_{13} product as a spherical top. The quantum results, which allow for or neglect tunnelling through the centrifugal barrier, are also shown besides the classical result.

steps in Γ appearing at values of ε_{tr} where J_r^{max} itself becomes a multiple of $\hbar$. The 10% difference in rotational constants used in these two calculations, as inferred from Figure 2, has a marginal influence on the rotational densities, hence our choice to neglect the variations of B with internal energy in the product cluster.

Taking now tunneling effects into account, the rotational density shows more continuous variations just before J_r^{max} increases by one $\hbar$, because the phase integral is low in magnitude only in this vicinity. Despite these qualitative differences, the quantum rotational density seems poorly altered by tunneling.

3. Product Angular Momentum. Phase space theory provides useful insight into the angular momentum of the product cluster, and performs equally well against classical simulations as for energetic properties.[40,41] The unnormalized probability distribution that a dissociation event leaves a product cluster with angular momentum J_r is[41]

$$P_r(J_r;E) = 2J_r \int_{\varepsilon_{tr}^{min}}^{E-E_0} \Omega_n(E - E_0 - \varepsilon_{tr})\, d\varepsilon_{tr} \qquad (19)$$

for a classical system. Here we have denoted $\varepsilon_{tr}^{min} = BJ_r^2 + \varepsilon^{\dagger}(J_r)$ the minimum rotational energy compatible with energy and angular momentum constraints.

The corresponding quantum expression is modified in two ways, namely, the discretization of J_r (associated with the semiclassical replacement of J_r^2 by $J_r(J_r + 1)$ in rotational energies), and the contribution of tunneling through the centrifugal barrier. The latter effect allows kinetic energies released to lie below ε_{tr}^{min} through the weighting function χ:

$$P_r(J_r;E) = (2J_r + 1)\times \left[\int_{BJ_r(J_r+1)}^{\varepsilon_{tr}^{min}} \chi(\varepsilon_{tr},J_r)\, \Omega_n(E - E_0 - \varepsilon_{tr})\, d\varepsilon_{tr} + \int_{\varepsilon_{tr}^{min}}^{E-E_0} \Omega_n(E - E_0 - \varepsilon_{tr})\, d\varepsilon_{tr} \right] \qquad (20)$$

Note again that ε_{tr} can never be lower than $BJ_r(J_r+1)$ even when tunneling is included; hence the first integral in eq 20 generally has a very narrow range.

The above expressions are used below to calculate the statistical average $\langle J_r \rangle$ of the distributions in the classical and quantum regimes.

III. Results and Discussion

Phase space theory has been used to calculate the absolute evaporation rates, the average (rotational + translational) kinetic energy released, and the average product angular momentum as a function of excess energy in the parent cluster. Temperature turns out to be a complementery control parameter to unravel the specific quantum effects, and it will be discussed as well, especially in the case of larger clusters for which the calculations were restricted to harmonic models.

A. Energy-Resolved Evaporation in Ne_{14}. We first consider the case of unimolecular evaporation in Ne_{14}, for which anharmonic densities of states have been determined for both the classical and quantum systems using the methods described in section II. Harmonic calculations have also been carried out for comparison. Here and in the following, the harmonic approximation means that only the lowest-energy structure was considered in the evaluation of vibrational state densities.

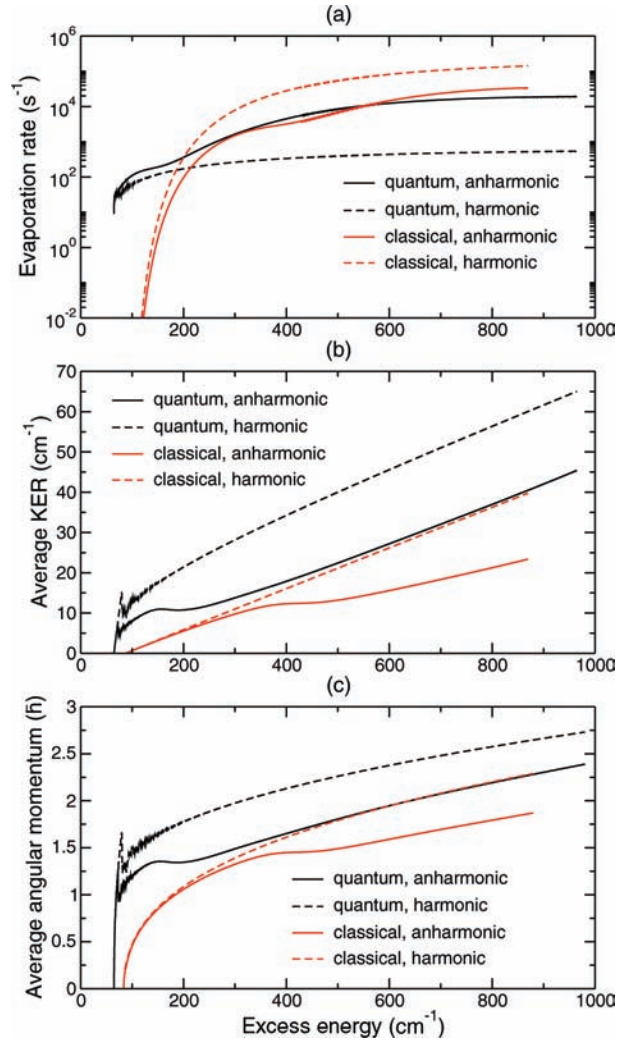

Figure 4. Predictions of phase space theory for the unimolecular evaporation of Ne_{14} into Ne_{13} + Ne as a function of internal energy, assuming quantum or classical treatments, and harmonic or anharmonic vibrational state densities: (a) evaporation rates; (b) average kinetic energy (translational + rotational) released; (c) average angular momentum of the product cluster.

The variations of k, $\langle \varepsilon_{tr} \rangle$, and $\langle J_r \rangle$ with excess energy E are represented in Figure 4. For the classical case, the rate constant and average KER show comparable behavior, as obtained previously for argon by Weerasinghe and Amar.[39] The general behavior of these properties is strongly affected by the quantum or classical treatment, especially at low energies. For instance, the classical rate can take arbitrarily low values and diverges when E reaches the dissociation energy E_0 from above. In contrast, the sum of states $W(E \rightarrow E_0)$ is limited by the vibrational density being always higher than 1/120 (corresponding to the point group of the highest possible symmetry, namely icosahedron) except when it is strictly zero, as in forbidden states. Classical densities and sums of vibrational states also grow faster with energy than their quantum counterparts, and this reflects on the evaporation rates. This explains why the quantum rates are generally higher than the classical rates at low energies, while they become lower at high energies.

Anharmonicity primarily affects the high-energy variations, and the rates are essentially close to the harmonic value near the dissociation threshold. However, anharmonicities have a much larger influence in the quantum case, as judged from the three properties considered here: the deviations from harmonic

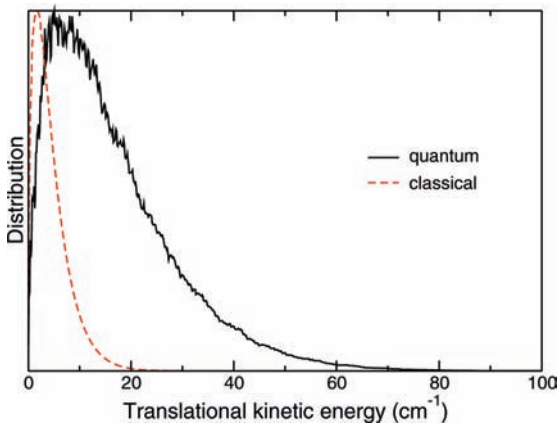

Figure 5. Distribution of translational kinetic energies released upon evaporation of Ne_{14}, at a fixed excess energy of 125 wavenumbers above the dissociation limit, assuming a quantum or a classical description, with anharmonic state densities.

behavior are seen at excess energies above about 300 cm^{-1} in the classical system, but both $\langle \varepsilon_{tr} \rangle$ and $\langle J_r \rangle$ deviate from their harmonic limit already a few wavenumbers above E_0. A significant difference between the classical and quantum curves lies in the qualitative effects of anharmonicity, which significantly increase the dissociation rate only in the quantum case. The decrease found in classical systems is consistent with the previous study by Weerasinghe and Amar.[39] We believe that this marked difference may come from some unsufficient sampling of the landscape of Ne_{14} with the superposition method, which despite reproducing the reference heat capacity does contain some errors in the estimated weights $w_n^{(\alpha)}$. However, the two harmonic results, where only the lowest-energy isomer is taken into account in the vibrational density of states, also show a strong difference that cannot be explained by sampling issues. This emphasizes that the interplay between quantum and anharmonicity effects is probably more subtle for these neon clusters than it is for more semiclassical systems such as aluminum clusters.[40] More generally, the results of Figure 4 suggest that these statistical observables are highly sensitive to the details of the vibrational densities, especially their strong fluctuations in the low-energy quantum regime. On a side note, the quantum anharmonic and classical harmonic results are found to be very similar for both the average KER and angular momentum. This fortuitous agreement only reflects some compensation between zero-point and anharmonic effects, which tend to increase and decrease, respectively, these two quantities.

The melting transition in the product cluster has clear signatures on all the three observables, not only in the classical cluster (near $E \approx 450$ cm^{-1} excess energy) but also in the quantum cluster (near $E \approx 200$ cm^{-1}). This further emphasizes the interplay between thermal equilibrium properties and dissociation properties.[39] The reduced melting energy found in the quantum case is consistent with previous studies in the canonical ensemble,[52−56] even though it will be more clearly evidenced when temperature is chosen as the control variable (see below).

The average KER and product angular momentum are significantly higher in the quantum system. This is a manifestation of the scarcity of vibrational states at low energies above the dissociation limit, low kinetic energy values becoming quantum mechanically forbidden in the integrals of eqs 4 and 5. This pure microcanonical effect is imposed by total energy constraints and can also be seen on the translational KER distributions. Figure 5 shows a typical such distribution at a moderate excess energy $E - E_0 = 125$ cm^{-1}. At this energy, quantum fluctuations have a major influence on energy distributions, whereas the classical distribution shows an expected smooth, Boltzmann-like shape. Even though translational energies are not explicitly quantified in our model, both vibrational and rotational energies are, and Figure 5 retains some signature of the ruggedness of the product vibrational density. The much broader support of the quantum distribution, which extends over 20 wavenumbers at half-width (versus about 8 cm^{-1} in the classical case), again illustrates the very low number of available vibrational states in the quantum case: most of the excess energy is converted into translational and rotational kinetic energies between the two products Ne_{13} and Ne.

The quantum mechanical treatment of phase space theory leads to important differences with the classical description for all properties considered so far. These differences are essentially caused by the low-energy fluctuating parts of the vibrational densities of states, which could not be captured by semiempirical corrections such as those based on the Pitzer−Gwinn approximation. They also convey a strong contrast between the microcanonical ensembles of the classical and quantum systems. This may be misleading in the case of gas-phase experiments on clusters which are often thermalized in a heat bath before being released into vacuum for selection and detection.

B. Temperature-Resolved Evaporation in Ne_{14}. All statistical properties $O(E)$ computed as a function of total energy have been recalculated for parent clusters in contact with a thermostat, using the appropriate Laplace transform of the microcanonical quantities with the parent density of states similar to eqs 10 and 11. The results of numerical quadratures are shown in Figure 6 for the Ne_{14} cluster described classically and quantum mechanically, assuming harmonic or anharmonic vibrational densities. The transformation into canonical properties has the immediate consequence of washing out low-energy quantum fluctuations. The quantum and classical values are now much closer to each other for the rates, the average KER and product angular momentum. The remaining signatures of quantum effects are found at low temperature as the nondiverging rate constants and much softer increases in $\langle \varepsilon_{tr} \rangle$ and $\langle J_r \rangle$. These latter variations mimic the softer behavior of the quantum caloric curve of the cluster, further indicating how equilibrium properties have imprints in dissociation observables also in the canonical ensemble.[39] In particular, the melting transition found near 10 K (classical system) and 9 K (quantum system, see the inset of Figure 1) occurs through inflections in the dissociation rate and the average KER close to these temperatures. However, with respect to the microcanonical case, anharmonicities now have a rather reduced impact, even in the classical cluster. This behavior results from the conjunction of two factors. First, the thermal distributions are broader and extend to higher energies in the anharmonic case. Second, the considered observables increase with energy in the microcanonical ensemble. Upon canonical averaging, anharmonic observables are much higher when anharmonicities are included.

Phase space theory provides the distributions of kinetic energies released and angular momenta of the product and can be straightforwardly used to estimate the vibrational energy ε_v remaining in the product after dissociation. Since $\varepsilon_v = E - E_0 - \varepsilon_{tr}$, the microcanonical probability of finding ε_v is simply proportional to $\Omega_n(\varepsilon_v) \times \Gamma(E - E_0 - \varepsilon_{vib})$. The distributions of vibrational energy in the Ne_{13} product after unimolecular dissociation are represented in Figure 7, for a parent Ne_{14} cluster assumed to be thermalized at 10 K, and with anharmonic vibrational densities. On this figure we also represented the

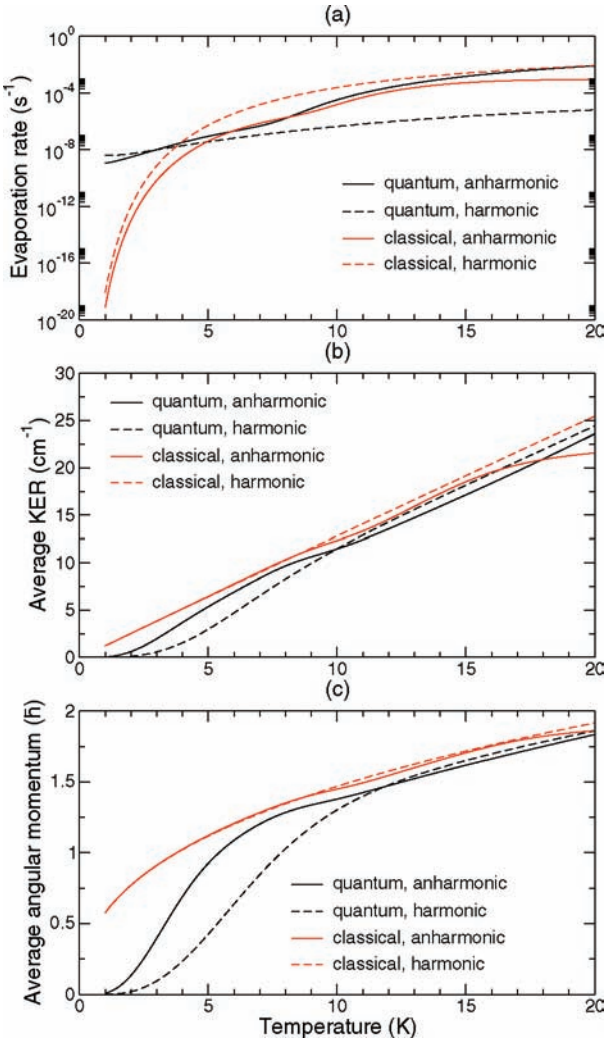

Figure 6. Predictions of phase space theory for the unimolecular evaporation of Ne_{14} into Ne_{13} + Ne as a function of canonical temperature, assuming quantum or classical treatments, and harmonic or anharmonic vibrational state densities: (a) evaporation rates; (b) average kinetic energy (translational + rotational) released; (c) average angular momentum of the product cluster.

corresponding thermal energy distributions in the parent at this same temperature. These distributions have comparable widths, but their centers differ due to many vibrational degrees of freedom being poorly occupied in the quantum case. This manifestation of strong delocalization, even at such a moderate temperature, can be seen on the distribution of vibrational energies in the product cluster. However, the quantum curve surprisingly shifts by 50 wavenumbers toward higher energies with respect to the parent distribution, whereas the classical distribution does not change much. This peculiarity suggests some evaporative heating, as was recently found in a theoretical study on classical 55-atom rare-gas clusters.[42] It is then a strong indication of a backbending in the microcanonical caloric curve of the quantum cluster, while the classical LJ_{13} cluster is known *not* to exhibit such a behavior.

C. Temperature from the KER Distribution. The connection between dissociation observables and equilibrium thermodynamical properties can be explicited further by considering the distribution of translational kinetic energies released.[33,34] Expanding the vibrational density in the integral of eq 5 leads to the well-known relation $P_t(E,\varepsilon_t) \propto \varepsilon_t^{2/3} \exp(-\varepsilon_t/k_B T_\mu)$ between the translational KER distribution and the microcanonical temperature $T_\mu = (\partial \ln \Omega_n/k_B \partial E)^{-1}$ of the product cluster. This

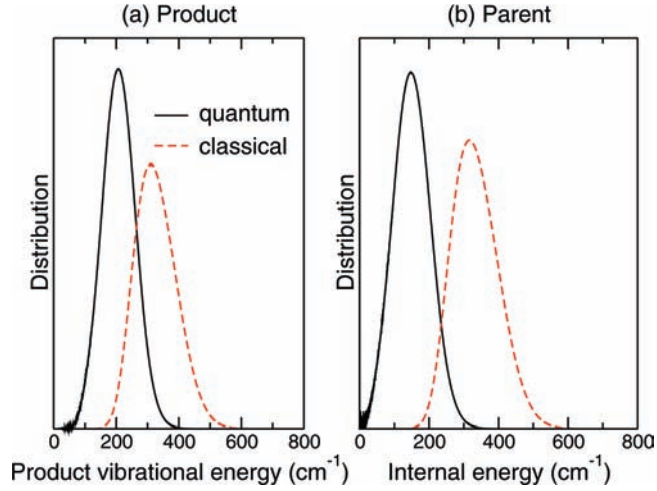

Figure 7. Left panel: distribution of vibrational energy remaining in the Ne_{13} product, for a parent Ne_{14} thermalized at 10 K. Right panel: thermal distribution of internal energy in Ne_{14} at 10 K. For both panels, the results obtained using quantum and classical treatments are shown. For both panels, energies are measured relative to the zero-point value.

relation was tested against the true microcanonical temperature computed by independent simulations in small neutral and cationic argon clusters.[34] In particular, it was suggested to correct for finite size and angular momentum effects in the expansion, replacing the previous exponential form by[34]

$$P_t(E,\varepsilon_t) \propto \left[1 - \exp\left(-\frac{\varepsilon_t^{2/3}}{\Lambda k_B T_\mu}\right)\right]\left[1 - \frac{k_B}{2C}\left(\frac{\varepsilon_t}{k_B T_\mu}\right)^2\right] \times \exp\left(-\frac{\varepsilon_t}{k_B T_\mu}\right) \quad (21)$$

in which C denotes the heat capacity of the cluster. We have calculated the microcanonical temperature $T_\mu(E)$ for the Ne_{13} cluster by direct numerical differentiation of the vibrational density of states, for both the quantum and classical systems. Distributions of translational kinetic energies released by the evaporation from Ne_{14} have also been calculated from phase space theory, using eq 5 above. To facilitate the interpretation of the results, quantum effects have only been included in the vibrational densities, and the angular momentum variables were treated classically. For each calculation at fixed excess energy, the KER distribution was fitted using the previous expression of eq 21, using the known value for Λ and assuming $C = (3n - 6)k_B$. The caloric curves $T_\mu^{fit}(E)$ extracted from this numerical procedure are shown in Figure 8 and compared with the microcanonical equilibrium temperatures. For the classical cluster, the present results are consistent with our previous study on argon clusters[34] and illustrate that the combination of finite-size and angular momentum corrections in eq 21 further improve the agreement between the microcanonical temperature and the KER-extracted value. The error in temperature determination is about 10% and is maximum near the melting energy range.

The microcanonical caloric curve of the quantum cluster is significantly affected by quantum fluctuations in the vibrational density of states at low energy, which blur any signature of the solidlike−liquidlike phase change. Much of this noise is magnified by the numerical derivative procedure involved in $T_\mu(E)$. The temperature obtained from adjusting the translational KER distribution follows a much smoother behavior, which even

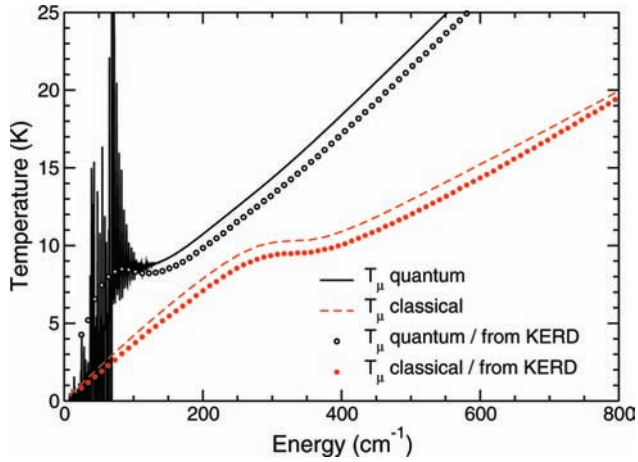

Figure 8. Microcanonical temperature of Ne_{13} as a function of its excess energy, obtained from the vibrational density of states (solid and dashed lines), or from fitting the translational kinetic energy released distribution to a modified Arrhenius form (symbols).

allows the detection of a melting region at excess energies in the 100−150 cm^{-1} range, associated with a temperature of about 8 K. Interestingly, the inflection in the quantum caloric curve is strong enough for a backbending to emerge, whereas the microcanonical heat capacity remains positive in the classical cluster. This confirms the suggestion that quantum delocalization might enhance backbending effects in atomic clusters.[80]

The present agreement between the microcanonical caloric curve and the temperature inferred from the KER distributions might further improve by adjusting the heat capacity C to more realistic values in eq 21, especially in quantum systems where C may be quite low. In the presence of a backbending, C might also diverge, making the fitting procedure useless. However, the simple approximation of considering C as a constant already provides an original but efficient method to determine practical caloric curves and to clear them from some inherent quantum noise.

D. Larger Clusters. Owing to an accumulation of low-frequency modes, the magnitude of quantum effects is expected to decrease with increasing cluster size. We have repeated the previous PST calculations for two clusters whose unimolecular dissociation products correspond to the next icosahedral magic series, namely, Ne_{56} and Ne_{148}. For these systems, only harmonic vibrational densities have been considered for simplicity. Sampling the energy landscape of these clusters remains feasible;[50] however, in the absence of any reference calculation for the quantum systems, we have not dared estimating anharmonic coefficients. The results of this section are thus aimed at providing trends.

The dissociation rate, average KER, and angular momentum product are represented in Figure 9 as a function of temperature in the parent cluster, for the three cluster sizes. Both classical and quantum properties are shown, except for the average KER where the classical curves, which give similar straight lines,[39] are omitted for clarity. Average properties are easier to discuss first, using simple analytic results available for classical harmonic clusters. The microcanonical KER for such systems varies with excess energy as $\langle\varepsilon_{tr}\rangle(E) \approx 2(E - E_0)/(3n - 7)$, where n is the size of the parent cluster.[39,81] This leads to a simple expression in the canonical ensemble, namely $\langle\varepsilon_{tr}\rangle(T) = 2[(3n - 3)k_BT - E_0]/(3n - 7)$. Hence the slope of the KER with temperature increases slowly with increasing n and converges to $2k_B$, which is close to the observed behavior in Figure 9 at high temperatures $T > 10$ K. Similarly, from eq 19

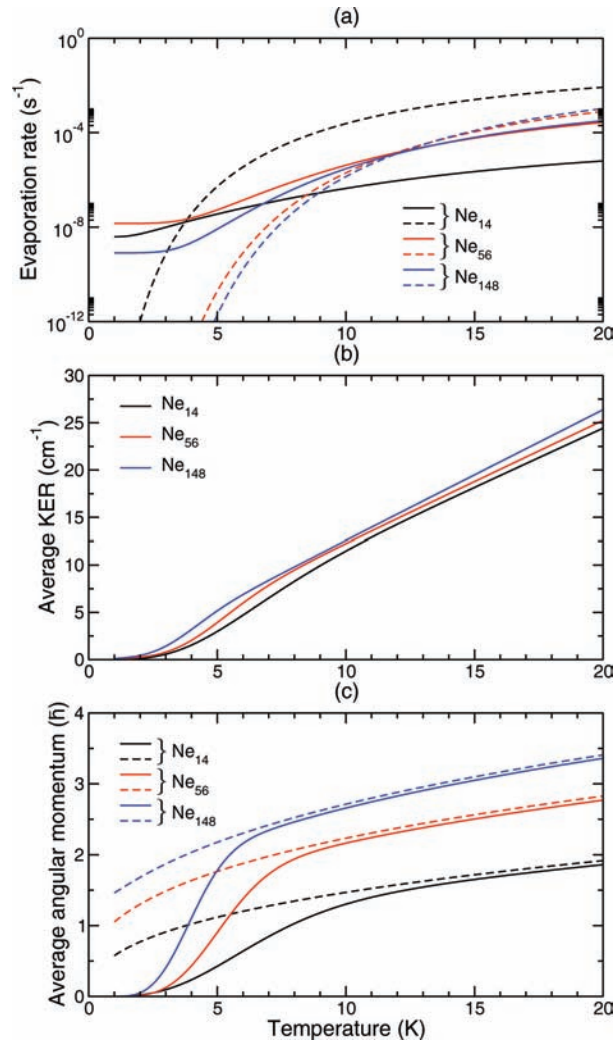

Figure 9. Predictions of phase space theory for the unimolecular evaporation of Ne_{56} and Ne_{148} as a function of canonical temperature, assuming quantum or classical treatments, and harmonic vibrational state densities: (a) evaporation rates; (b) average kinetic energy (translational + rotational) released; (c) average angular momentum of the product cluster. Solid lines refer to quantum systems, whereas dashed lines, when present, refer to classical systems. Those have been omitted from panel (b) for clarity.

the microcanonically averaged angular momentum product varies for an harmonic classical cluster as $\langle J_r\rangle(E) \approx [(E - E_0)/B]^{1/2}$ at low energies, leading to a $(k_BT/B)^{1/2}$ behavior as a function of temperature. This explains how the different curves in Figure 9c scale with cluster size, since in a first approximation $B(n) \propto n^{-5/3}$. The quantum properties follow comparable variations. The temperatures at which the quantum and classical averages meet decrease with increasing cluster size. This corroborates the appearance of many softer vibrational modes, which makes larger clusters behaving in a more classical fashion at fixed temperature.

Finally, the dissociation rates are far more affected by the classical or quantum nature of the clusters than by their size. In particular, as was already the case for the Ne_{14} system but in contrast with average properties, the classical and quantum rates do not converge to each other at high temperatures. Since the rotational densities of states have the same magnitude, this discrepancy must be caused by uncertainties in the absolute densities of states, especially acute due to the different methods used to calculate them in classical and quantum systems. These differences are less marked for Ne_{148} and Ne_{56} but remain clearly

visible after the crossing of all the corresponding curves near $T = 10$ K. More remarkable is the qualitative influence of quantum effects on the nontrivial variations of the dissociation rates that often show inflections at low temperatures even though both parent and product clusters are described as sets of harmonic oscillators. The complex variations and temperature-dependent ordering between the dissociation rates found for quantum systems cannot be explained by simple scaling arguments, and this conclusion is also valid for classical systems, despite the possible shift in the quantum versus classical values. Absolute rates thus depend on the precise details of both parent and product clusters, especially on the distributions of vibrational frequencies. They are also affected by the different symmetry factors in the parent, which differ between Ne_{148}, Ne_{56}, and Ne_{14}. Following the conclusions of Weerasinghe and Amar,[39] average properties and equilibrium distributions appear as much robust quantities to separate the relative influences of the various parameters entering these calculations.

E. Discussion. The difficulty in interpreting the energy-resolved results lie in the qualitatively different vibrational distributions, which exhibit strong (nonmonotonic) fluctuations in quantum systems but display smooth and always increasing variations in classical systems. In addition, only a few vibrational states are allowed in quantum clusters until their total energy is sufficient. Hence the evaporation products may be emitted vibrationally cold, and even nearly frozen, but are still capable of carrying some significant momenta. The picture emerging in the canonical ensemble strongly contrasts with the previous microcanonical one, because the parent excess energy distribution is itself much narrower at low energies, thus restoring a more intuitive behavior in the dissociation observables.

So far we have not discussed the influence of quantum tunneling on the computed properties. This phenomenon enters the theory only via the rotational densities of states but even then has a minor contribution. All calculations for the quantum systems have been repeated by canceling the tunneling probability χ, and the results appear indistinguishable. Furthermore, using the classical rotational densities together with quantum vibrational densities leaves the rate constants and kinetic energy release distributions essentially unchanged. Angular momentum observables are only affected due to their discrete character in units of $\hbar$, becoming slightly lower. Looking at the shape of the rotational density in Figure 3, this result should not be taken as a surprise. Except for the absolute rate constants, the statistical properties for such rather large systems should be mainly controlled by the number of rotational degrees of freedom via power law expressions,[90] the centrifugal energies being only small magnitude corrections. Tunneling through the centrifugal barrier is itself a rare event for the present clusters but could be enhanced in smaller systems involving lighter species. In this case the range of angular momenta would be reduced, the phase integral would be significantly higher, and the combined effect on the rotational density might become visible on the statistical properties.

IV. Summary and Conclusions

Neon clusters have a particular status as weakly bound systems exhibitting a behavior intermediate between fully quantum (as in helium) or mainly classical (as in heavy rare gases). This status makes them suitable for fundamental studies on the multidimensional vibrational dynamics using ideas from the semiclassical realm. In the present work, the unimolecular dissociation of neon clusters containing 14, 56, and 148 atoms has been investigated in the framework of phase space theory in its orbiting transition state version, paying a particular attention to the role of quantum effects. The vibrational densities of states have been calculated for these clusters and their dissociation products using dedicated simulation schemes based on Monte Carlo methods for classical systems, and the superposition approximation in the quantum case. Full anharmonicities have been included in smaller clusters. Semiclassical discretization of angular momentum, as well as quantum tunneling through the centrifugal barrier, were found to have only a limited effect on most properties, whereas the quantum description of vibrational states is crucial in determining the energy- and temperature-dependent properties.

Our work confirms the previous conclusions of Weerasinghe and Amar[39] about the possibility of using dissociation observables as a way to acess thermodynamical equilibrium properties, even for probing possible phase changes. The depression in the melting point of Ne_{13} due to quantum effects, for instance, was found to have a quantitative signature on the average KER, product angular momenta, and even the rate constant. Note, however, that the latter is much harder to interpret in general since it involves the parent and product properties in equal importance. Combinations of backbendings in the vibrational state densities of both the parent and product could well lead to complex, nonmonotonic variations of the microcanonical rate constant with increasing energy.

Quantization of vibrations scrambles the relation between energy E and microcanonical temperature T_μ. However, when the translational KER distribution is used to estimate T_μ, much of these fluctuations are washed out from the fitting procedure, and a smoother caloric curve emerges. In particular, and contrary to the classical case, the melting transition occurs in the quantum Ne_{13} with a clear backbending in the microcanonical temperature extracted from the KER distribution. Larger systems should behave more and more classically due to an accumulation of low-frequency modes, and backbendings should be seen even easier in Ne_{55} and Ne_{147}, quantum fluctuations being significant on the microcanonical curves only at very low energies.

For the present systems, the magnitude of quantum effects lies beyond the capabilities of most corrective approaches based on Pitzer−Gwinn approximations and alike. The superposition approximation used here to estimate vibrational densities should itself become exceedingly crude for dealing with lighter elements such as hydrogen. Microcanonical path-integral techniques might then become the method of choice.

It would be useful to apply the methods developed in this article to ionized neon clusters, for their greater experimental relevance in mass spectrometry studies.[91] Cationic rare-gas clusters display a much richer structural, dynamical, and thermodynamical behavior than their neutral counterparts, due to the formation of a covalent ionic core solvated by neutral atoms bound to the core via polarization and dispersion forces.[92−96] The stronger binding in these clusters make them more classical, but the number of weak bonds increases quickly with cluster size. The resulting species offer an intermediate situation with intriguing properties, which might be more amenable to successful modeling by the aforementioned quantum corrective approaches to classical treatments.

The main limitation of the results obtained here is their lack of support from explicit, atomistic simulation of the evaporation process. Among the various methods quoted in the introductory section, several of them stand out as promising candidates to address the long-time quantum dynamics of many-body systems on highly anharmonic energy landscapes. In the near future, further methodological improvements, together with advances

in computer algorithms and hardware, should enable fruitful comparison with the present findings.

Acknowledgment. Useful discussions with Prof. F. G. Amar are gratefully acknowledged. We also thank GDR 2758 "Thermodynamique et Fragmentation des Systèmes Complexes" for financial support, and the Pôle Scientifique de Modélisation Numérique for a generous allocation of computer resources.

Appendix: Rotational Constants in the Superposition Approximation

In the superposition approximation, the effective rotational constant is obtained from the spherical average of the principal momenta of inertia of an effective inertia tensor $\mathbf{I}(T)$:

$$\mathbf{I}(T) = \frac{1}{Z(T)} \sum_{\alpha} \langle \mathbf{I}_{\alpha} \rangle (T) S_n^{(\alpha)} Z_n^{(\alpha)}(T) \tag{22}$$

where $Z(T) = \Sigma_{\alpha} S_n^{(\alpha)} Z_n^{(\alpha)}(T)$ is the total partition function of the system and $\langle \mathbf{I}_{\alpha} \rangle (T)$ is the thermally averaged inertia tensor of isomer α at temperature T. The quantum partition function is the Laplace transform of the density of states $\Omega_n^{(\alpha)}(E)$, and in the classical case we use an anharmonic perturbative expansion at first order.[84]

The 3×3 matrix $\langle \mathbf{I}_{\alpha} \rangle (T)$ is calculated at the harmonic level. The transformation from Cartesian coordinates $\mathbf{R} = \mathbf{R}_{\alpha} + \delta\mathbf{R}$ to normal modes $\mathbf{Q}$ around the equilibrium geometry $\mathbf{R}_{\alpha}$ of isomer α involves the orthogonal matrix $\mathbf{W}$ such that $\delta\mathbf{R} = \mathbf{WQ}$. Upon this transformation each term of the $\mathbf{I}_{\alpha}$ tensor is expressed as a a linear combination of $Q_i Q_j$ products; hence $\langle \mathbf{I}_{\alpha} \rangle (T)$ is simply obtained from $\langle Q_i Q_j \rangle$ averages. Assuming harmonic wave functions yields

$$\langle Q_i Q_j \rangle (T) = \delta_{ij} \frac{\hbar}{2m\omega_{\alpha}^{(i)} \tanh \hbar\omega_{\alpha}^{(i)}/2k_B T} \tag{23}$$

where δ_{ij} stands for the Kronecker symbol. The classical expression is straightforwardly obtained as

$$\langle Q_i Q_j \rangle (T, \hbar \rightarrow 0) = \delta_{ij} \frac{k_B T}{m[\omega_{\alpha}^{(i)}]^2} \tag{24}$$

The $T \rightarrow 0$ limit of eq 23 also leads to a zero-point correction to the effective inertia tensor, which is sufficient to reduce the rotational constant by about 10% (see Figure 2).

References and Notes

(1) Kosloff, R. In *Dynamics of Molecular and Chemical Reactions*; Wyatt, R. E., Zhang, J. Z., Eds.; Dekker: New York, 1996; p 185. Kosloff, R. *Annu. Rev. Phys. Chem.* **1994**, *45*, 145.

(2) Bowman, J. M. *J. Chem. Phys.* **1978**, *68*, 608. Gerber, R. B.; Ratner, M. A. *Chem. Phys. Lett.* **1979**, *68*, 195. Ratner, M. A.; Gerber, R. B. *J. Phys. Chem.* **1986**, *90*, 20. McCoy, A. B. *Chem. Phys. Lett.* **1998**, *293*, 103. McCoy, A. B.; Wang, L.; Chen, F. *Faraday Discuss.* **2001**, *118*, 281.

(3) Meyer, H.-D.; Manthe, U.; Cederbaum, L. S. *Chem. Phys. Lett.* **1990**, *165*, 73. Manthe, U.; Meyer, H.-D.; Cederbaum, L. S. *J. Chem. Phys.* **1992**, *97*, 3199. Burghardt, I.; Meyer, H.-D.; Cederbaum, L. S. *J. Chem. Phys.* **1999**, *111*, 2927. Burghardt, I.; Nest, M.; Worth, G. A. *J. Chem. Phys.* **2004**, *119*, 5364.

(4) Cao, J. S.; Voth, G. A. *J. Chem. Phys.* **1994**, *100*, 5093; **1994**, *100*, 5106; **1994**, *101*, 6157.

(5) Craig, I. R.; Manolopoulos, D. E. *J. Chem. Phys.* **2004**, *121*, 3368. **2005**, *123*, 034102.

(6) Van Voorhis, T.; Heller, E. J. *Phys. Rev. A* **2002**, *66*, 050501; *J. Chem. Phys.* **2003**, *119*, 12153. Novaes, M.; de Aguiar, M. A. M. *Phys. Rev. A* **2005**, *72*, 032105. Sawada, S.; Heather, R.; Jackson, B.; Metiu, H. *Chem. Phys. Lett.* **1989**, *155*, 77. Kay, K. G. *J. Chem. Phys.* **1989**, *91*, 170. Ben-Nun, M.; Martínez, T. *Adv. Chem. Phys.* **2002**, *121*, 439. Shalashilin, D. V.; Jackson, B. *Chem. Phys. Lett.* **1998**, *291*, 143. Wu, Y.; Batista, V. S. *J. Chem. Phys.* **2003**, *118*, 6720. Kassal, I.; Jordan, S. P.; Love, P. J.; Mohseni, M.; Aspuru-Guzik, A. *Proc. Natl. Acad. Sci. U.S.A.* **2008**, *105*, 18681.

(7) Lopreore, C. L.; Wyatt, R. E. *Phys. Rev. Lett.* **1999**, *82*, 5190. Trahan, C. J.; Wyatt, R. E. *J. Chem. Phys.* **2003**, *119*, 7017. Makri, N. *J. Phys. Chem. A* **2004**, *108*, 806.

(8) Makri, N. *Annu. Rev. Phys. Chem.* **1999**, *50*, 167.

(9) Derrickson, S. W.; Bittner, E. R. *J. Phys. Chem. A* **2007**, *111*, 10345.

(10) Heller, E. J. *J. Chem. Phys.* **1975**, *62*, 1544. **1976**, *64*, 63.

(11) Coalson, R. D.; Karplus, M. *J. Chem. Phys.* **1990**, *93*, 3919.

(12) Buch, V. *J. Chem. Phys.* **2002**, *117*, 4738.

(13) Ben-Nun, M.; Martínez, T. J. *Adv. Chem. Phys.* **2002**, *121*, 439.

(14) Pak, M. V.; Hammes-Schiffer, S. *Phys. Rev. Lett.* **2004**, *92*, 103002.

(15) Gulmen, T. S.; Sibert, E. L. *J. Phys. Chem. A* **2004**, *108*, 2389.

(16) Sterling, M.; Li, Z.; Apkarian, V. A. *J. Chem. Phys.* **1995**, *103*, 5679.

(17) Thoss, M.; Wang, H. *Annu. Rev. Phys. Chem.* **2004**, *55*, 299.

(18) Miller, W. H.; Zhao, Y.; Ceotto, M.; Yang, S. *J. Chem. Phys.* **2003**, *119*, 1329. Peters, B.; Bell, A. T.; Chakraborty, A. *J. Chem. Phys.* **2004**, *121*, 4461.

(19) Horenko, I.; Weiser, M.; Schmidt, B.; Schütte, C. *J. Chem. Phys.* **2004**, *120*, 8913. Riga, J. M.; Martens, C. C. *J. Chem. Phys.* **2004**, *120*, 6863. Heatwole, E. M.; Prezhdo, O. V. *J. Chem. Phys.* **2005**, *122*, 234109. Saha, R.; Ovchinnikov, M. *J. Chem. Phys.* **2006**, *124*, 204112.

(20) Slavíček, P.; Jungwirth, P.; Lewerenz, M.; Nahler, N. H.; Fárník, M.; Buck, U. *J. Phys. Chem. A* **2003**, *107*, 7743.

(21) Grossmann, F. *J. Chem. Phys.* **2006**, *125*, 014111.

(22) Jungwirth, P.; Gerber, R. B. *Chem. Rev.* **1999**, *99*, 1583.

(23) Path-integral methods in the microcanonical ensemble have been suggested by a few authors, but they have been applied so far only to model low-dimensional systems. See for instance: Freeman, D. L.; Doll, J. D. *J. Chem. Phys.* **1994**, *101*, 848. Lawson, J. D. *Phys. Rev. E* **2000**, *61*, 61.

(24) Bowman, J. M.; Gazdy, B.; Sun, Q. *J. Chem. Phys.* **1989**, *91*, 2859.

(25) Miller, W. H.; Hase, W. L.; Darling, C. L. *J. Chem. Phys.* **1989**, *91*, 2863.

(26) Seeley, G.; Keyes, T. M. *J. Chem. Phys.* **1989**, *91*, 5581.

(27) Truhlar, D. G.; Muckerman, J. T. In *Atom-Molecule Collision Theory*; Bernstein, R. B., Ed.; Plenum: New York, 1979.

(28) Xu, B.-C.; Stratt, R. M. *J. Chem. Phys.* **1990**, *92*, 1923. Adams, J. E.; Stratt, R. M. *J. Chem. Phys.* **1990**, *93*, 1332.

(29) Stock, G.; Thoss, M. *Phys. Rev. Lett.* **1997**, *78*, 578. Stock, G.; Müller, U. *J. Chem. Phys.* **1999**, *111*, 65.

(30) McCormack, D. A.; Lim, K. F. *Phys. Chem. Chem. Phys.* **1999**, *1*, 1.

(31) Bonhommeau, D.; Truhlar, D. G. *J. Chem. Phys.* **2008**, *129*, 014302.

(32) Klots, C. E. *Z. Phys. D: At., Mol. Clusters* **1987**, *5*, 83.

(33) Hansen, K.; Näher, U. *Phys. Rev. A* **1999**, *60*, 1240.

(34) Calvo, F.; Parneix, P.; Gadéa, F.-X. *J. Phys. Chem. A* **2006**, *110*, 1561.

(35) Schmidt, M.; Kusche, R.; Kronmüller, W.; von Issendorff, B.; Haberland, H. *Phys. Rev. Lett.* **1997**, *79*, 99.

(36) Breaux, G. A.; Benirschke, R. C.; Sugai, T.; Kinnear, B. S.; Jarrold, M. F. *Phys. Rev. Lett.* **2003**, *91*, 215508.

(37) Róman, C. E.; Garzón, I. L. *Z. Phys. D: At., Mol. Clusters* **1991**, *20*, 163.

(38) Smith, R. W. *Z. Phys. D: At., Mol. Clusters* **1991**, *21*, 57.

(39) Weerasinghe, S. A.; Amar, F. G. *J. Chem. Phys.* **1993**, *98*, 4967.

(40) Peslherbe, G. H.; Hase, W. L. *J. Chem. Phys.* **1996**, *104*, 9445; *J. Phys. Chem. A* **2000**, *104*, 10556.

(41) Calvo, F.; Parneix, P. *J. Chem. Phys.* **2003**, *119*, 256. Parneix, P.; Calvo, F. *J. Chem. Phys.* **2003**, *119*, 9469. Calvo, F.; Parneix, P. *J. Chem. Phys.* **2004**, *120*, 2780; **2004**, *121*, 11088.

(42) Calvo, F.; Parneix, P. *J. Chem. Phys.* **2007**, *126*, 34309.

(43) Nikitin, E. *Theor. Exp. Chem.* **1965**, *1*, 83. **1965**, *1*, 275.

(44) Pechukas, P.; Light, J. C. *J. Chem. Phys.* **1965**, *42*, 3281. Light, J. C. *Discuss. Faraday Soc.* **1967**, *44*, 14.

(45) Klots, C. E. *J. Phys. Chem.* **1971**, *75*, 1526; *Z. Naturforsch. A* **1971**, *27*, 553; *Adv. Mass Spectrom.* **1973**, *6*, 9696.

(46) Marcus, R. A. *J. Chem. Phys.* **1975**, *62*, 1872.

(47) Chesnavich, W. J.; Bowers, M. T. *J. Am. Chem. Soc.* **1976**, *98*, 8301; *J. Chem. Phys.* **1977**, *66*, 2306 *J. Am. Chem. Soc.* **1977**, *99*, 1705.

(48) Brink, D. M.; Stringari, S. *Z. Phys. D: At., Mol. Clusters* **1990**, *15*, 257.

(49) Lehmann, K. K.; Dokter, A. M. *Phys. Rev. Lett.* **2004**, *92*, 173401.

(50) Calvo, F.; Doye, J. P. K.; Wales, D. J. *J. Chem. Phys.* **2001**, *114*, 7312.

(51) Deckman, J.; Frantsuzov, P. A.; Mandelshtam, V. A. *Phys. Rev. E* **2008**, *77*, 052102.

(52) Frantz, D. D.; Freeman, D. L.; Doll, J. D. *J. Chem. Phys.* **1992**, *97*, 5713.
(53) Chakravarty, C. *J. Chem. Phys.* **1995**, *102*, 956; **1995**, *103*, 10663.
(54) Neirotti, J. P.; Freeman, D. L.; Doll, J. D. *J. Chem. Phys.* **2000**, *112*, 3990.
(55) Predescu, C.; Sabo, D.; Doll, J. D.; Freeman, D. L. *J. Chem. Phys.* **2003**, *119*, 12119.
(56) Pahl, E.; Calvo, F.; Koçi, L.; Schwerdtfeger, P. *Angew. Chem., Int. Ed.* **2008**, *47*, 8207.
(57) Sese, L. M. *Mol. Phys.* **1993**, *78*, 1167.
(58) Solca, J.; Dyson, J.; Steinebrunner, G.; Kirchner, B.; Huber, H. *J. Chem. Phys.* **1998**, *108*, 4107.
(59) Wales, D. J. *Mol. Phys.* **1993**, *78*, 151.
(60) Watanabe, W.; Reinhardt, W. P. *Phys. Rev. Lett.* **1990**, *65*, 3301.
(61) Neirotti, J. P.; Calvo, F.; Freeman, D. L.; Doll, J. D. *J. Chem. Phys.* **2000**, *112*, 10340.
(62) Feynman, R. P.; Hibbs, A. R. *Quantum mechanics and path integrals*; McGraw-Hill: New York, 1965.
(63) Hüpper, B.; Pollak, E. *J. Chem. Phys.* **1999**, *110*, 11176.
(64) Berblinger, M.; Schlier, C. *J. Chem. Phys.* **1992**, *96*, 6834.
(65) Börjesson, L. E. B.; Nordholm, S.; Andersson, L. A. *Chem. Phys. Lett.* **1991**, *186*, 65.
(66) Wadi, H.; Pollak, E. *J. Chem. Phys.* **1999**, *110*, 8246.
(67) Parneix, P.; Nguyen-Thi, V.-O.; Bréchignac, Ph. *Chem. Phys. Lett.* **2002**, *357*, 78.
(68) Pitzer, K. S.; Gwinn, W. D. *J. Chem. Phys.* **1942**, *10*, 428.
(69) Rapacioli, M.; Calvo, F.; Joblin, C.; Parneix, P.; Spiegelman, F. *J. Phys. Chem. A* **2007**, *111*, 2999. Spiegelman, F.; Calvo, F. *Collect. Czech. Chem. Commun.* **2007**, *72*, 278.
(70) Doll, J. D. *Chem. Phys. Lett.* **1980**, *72*, 139.
(71) Isaacson, A. D.; Truhlar, D. G. *J. Chem. Phys.* **1981**, *75*, 4090. Isaacson, A. D.; Truhlar, D. G.; Scanlon, K.; Overend, J. *J. Chem. Phys.* **1981**, *75*, 3017.
(72) Stillinger, F. H.; Weber, T. A. *Phys. Rev. A* **1992**, *25*, 978.
(73) Doye, J. P. K.; Wales, D. J. *J. Chem. Phys.* **1995**, *102*, 9659.
(74) Calvo, F.; Doye, J. P. K.; Wales, D. J. *Chem. Phys. Lett.* **2002**, *366*, 176.
(75) Angelani, L.; Parisi, G.; Ruocco, G.; Viliani, G. *Phys. Rev. Lett.* **1998**, *81*, 4648. Sastry, S. *J. Phys.: Condens. Matter* **2000**, *12*, 6523. Middleton, T. F.; Wales, D. J. *J. Chem. Phys.* **2004**, *120*, 8134. Chowdary, J.; Keyes, T. *J. Phys. Chem. B* **2004**, *108*, 19786. Heuer, A.; Doliwa, B.; Saksaengwijit, A. *Phys. Rev. E* **2005**, *72*, 021503.
(76) Strodel, B.; Wales, D. J. *Chem. Phys. Lett.* **2008**, *466*, 105.
(77) Beyer, T.; Swinehart, D. *Commun. ACM* **1973**, *16*, 379. Stein, S.; Rabinovitch, B. *J. Chem. Phys.* **1973**, *58*, 2438.
(78) Noid, D. W.; Koszykowski, M. L.; Tabor, M.; Marcus, R. M. *J. Chem. Phys.* **1980**, *72*, 6169. Farantos, S. C.; Murrel, J. N.; Hajduk, J. C. *Chem. Phys.* **1982**, *68*, 109. Toselli, B. M.; Barker, J. R. *Chem. Phys. Lett.* **1989**, *159*, 499.
(79) Basire, M.; Parneix, P.; Calvo, F. *J. Chem. Phys.* **2008**, *129*, 081101.
(80) Calvo, F.; Parneix, P.; Basire, M. *J. Chem. Phys.*, in press.
(81) Engelking, P. C. *J. Chem. Phys.* **1986**, *85*, 3103; **1987**, *87*, 937.
(82) Frantsuzov, P. A.; Mandelshtam, V. A. *J. Chem. Phys.* **2004**, *121*, 9247.
(83) Frantsuzov, P. A.; Mandelshtam, V. A. Private communication.
(84) Calvo, F.; Doye, J. P. K.; Wales, D. J. *J. Chem. Phys.* **2001**, *115*, 9627.
(85) Klots, C. E. *J. Chem. Phys.* **1994**, *100*, 1035.
(86) Vogt, E.; Wannier, G. H. *Phys. Rev.* **1954**, *95*, 1190.
(87) Klots, C. E. *Chem. Phys. Lett.* **1971**, *10*, 422.
(88) Child, M. A. *Semiclassical Mechanics with Molecular Applications*; Clarendon Press: Oxford, U.K., 1991.
(89) Larregaray, P.; Bonnet, L.; Rayez, J.-C. *J. Phys. Chem. A* **2006**, *110*, 1552.
(90) Klots, C. E. *J. Chem. Phys.* **1976**, *64*, 4269.
(91) Märk, T. D.; Scheier, P. *Chem. Phys. Lett.* **1987**, *137*, 245. Parajuli, R.; Matt, S.; Echt, O.; Stamatovic, A.; Scheier, P.; Märk, T. D. *Chem. Phys. Lett.* **2002**, *352*, 288.
(92) Fieber, M.; Ding, A. M. G.; Kuntz, P. J. *Z. Phys. D: At., Mol. Clusters* **1992**, *23*, 171.
(93) Naumkin, F. Y.; Wales, D. J. *Mol. Phys.* **1998**, *93*, 633.
(94) Galindez, J.; Calvo, F.; Paska, P.; Hrivnak, D.; Kalus, R.; Gadéa, F. X. *Comput. Phys. Commun.* **2002**, *124*, 126, and references therein.
(95) Bonhommeau, D.; Viel, A.; Halberstadt, N. *J. Chem. Phys.* **2005**, *123*, 054316.
(96) Aquilanti, V.; Lombardi, A.; Gadéa, F. X.; Calvo, F. *J. Chem. Phys.* **2006**, *125*, 114307.

JP903282B